HHS Public Access

Author manuscript

Nat Med. Author manuscript; available in PMC 2015 May 01.

Published in final edited form as:

Nat Med. 2014 November ; 20(11): 1254–1262. doi:10.1038/nm.3700.

Cleavage of tau by asparagine endopeptidase mediates the neurofibrillary pathology in Alzheimer's disease

Zhentao Zhang[1,2], **Mingke Song**[3], **Xia Liu**[1], **Seong Su Kang**[1], **Il-Sun Kwon**[1], **Duc M. Duong**[4,5], **Nicholas T. Seyfried**[4,5], **William T. Hu**[4], **Zhixue Liu**[6], **Jian-zhi Wang**[7], **Liming Cheng**[8,9], **Yi E. Sun**[8], **Shan Ping Yu**[3], **Allan I. Levey**[4], and **Keqiang Ye**[1,9]

[1]Department of Pathology and Laboratory Medicine, Center for Neurodegenerative Diseases, Emory University School of Medicine, Atlanta, GA 30322, USA

[2]Department of Neurology, Renmin Hospital of Wuhan University, Wuhan 430060, China

[3]Department of Anesthesiology, Center for Neurodegenerative Diseases, Emory University School of Medicine, Atlanta, GA 30322, USA

[4]Department of Neurology, Center for Neurodegenerative Diseases, Emory University School of Medicine, Atlanta, GA 30322, USA

[5]Department of Biochemistry, Center for Neurodegenerative Diseases, Emory University School of Medicine, Atlanta, GA 30322, USA

[6]Key Laboratory of Nutrition and Metabolism, Institute for Nutritional Sciences, Shanghai Institutes for Biological Sciences, Chinese Academy of Sciences, Graduate School of the Chinese Academy of Sciences, Shanghai 200031, China

[7]Department of Pathophysiology, Key Laboratory of Ministry of Education of Neurological Diseases, Tongji Medical College, Huazhong University of Science and Technology, Wuhan, China

[8]Translational Center for Stem Cell Research, Tongji Hospital, Department of Regenerative Medicine, Tongji University School of Medicine, Shanghai 200065, China

Abstract

Neurofibrillary tangles (NFTs), composed of truncated and hyperphosphorylated tau, are a common feature of numerous aging-related neurodegenerative diseases including Alzheimer's disease (AD). However, the molecular mechanisms mediating tau truncation and aggregation

[9]To whom correspondence should be addressed (kye@emory.edu; limingcheng@tongji.edu.cn).

AUTHOR CONTRIBUTIONS

K.Y. conceived the project, designed the experiments, and wrote the manuscript. Z.Z. designed and performed most of the experiments. M. S. and S.P.Y. performed the electrophysiological experiments. X.L. prepared primary neurons and assessed with animal experiments. S.S.K performed the stereotaxic injection of virus. D.M.D. and N.T.S performed the mass spectrometry analysis. I.K. assisted with the molecular biology experiments. L.C., W.T.H. Z.L., J. W., Y.E.S., and A.I.L. designed the experiments, assisted with data analysis and interpretation and critically read the manuscript.

COMPETING FINANCIAL INTERESTRS

The authors declare no competing financial interests.

during aging remain elusive. Here we show that asparagine endopeptidase (AEP), a lysosomal cysteine proteinase, is activated during aging and proteolytically degrades tau, abolishes its microtubule assembly function, induces tau aggregation, and triggers neurodegeneration. AEP is upregulated and active during aging, and is activated in tau P301S transgenic mice and human AD brain, leading to tau truncation in NFTs. Deletion of AEP from tau P301S transgenic mice substantially reduces tau hyperphosphorylation, alleviates the synapse loss and rescues impaired hippocampal synaptic function and the cognitive deficits. Infection of uncleavable tau N255AN368A mutant rescues tau P301S-induced pathological and behavioral defects. Together, these observations indicate that AEP acts as a crucial mediator of tau-related clinical and neuropathological changes in neurodegenerative diseases. Inhibition of AEP may be therapeutically useful for treating tau-mediated neurodegenerative diseases.

INTRODUCTION

Alzheimer's disease (AD) is a progressive neurodegenerative disease characterized by two neuropathological hallmarks: extracellular senile plaque deposits, composed of amyloid beta (Aβ), and intracellular neurofibrillary tangles (NFTs), made of truncated and hyperphosphorylated tau. Tau-mediated neurodegeneration may result from the combination of toxic gains-of-function acquired by the aggregates and the detrimental effects that arise from the loss of the normal function(s) [1]. Tau is mainly expressed in neurons and abundant in the neuronal axons, regulating microtubule (MT) polymerization and stabilizing MT. Through alternative splicing, the *MAPT* gene yields six major isoforms [2]. While normal phosphorylation of tau controls the dynamics of MT, establishing neuronal polarity, axonal outgrowth and axonal transport [3–6], pathological hyperphosphorylation in disease severely interferes with tau's ability to regulate MT dynamics [7–9]. Hyperphosphorylated tau displays an increased propensity to form paired helical filaments (PHFs) *in vitro* and sequesters full-length tau and other microtubule associated proteins [10–12], indicating that hyperphosphorylation is a potent inducer of tau pathology. In AD, tau undergoes a number of other posttranslational modifications in addition to phosphorylation that contribute to the tau aggregation and disease pathology.

Tau is a substrate for various proteases. Tau can be cleaved by several caspases at Asp421. In AD brain, tau truncated at Asp421 is a component of NFTs, and Aβ induces this cleavage in cultured neurons [13–15]. In AD brain, calpain 1 and calpain 2 are abnormally activated [16]. Aβ treatment leads to activation of calpains and production of a 17 kDa fragment in neurons (tau45–230). Overexpression of tau45–230 induces neuronal apoptosis [17]. In addition to caspases and calpains, thrombin and cathepsins have also been implicated in processing tau [18–20]. However, many tau fragments found in AD are not well characterized and the proteases responsible for their generation have not all been identified. For instance, a 25–35 kDa tau fragment in the cerebrospinal fluid (CSF) has been used as an early marker of AD [21,22], but the proteases responsible for this cleavage event are unknown.

Mammalian asparagine endopeptidase (AEP), also known as legumain (LGMN), is a lysosomal cysteine protease that cleaves protein substrates on the C-terminal side of asparagine [23,24]. AEP activation is autocatalytic and requires sequential removal of C- and

N-terminal propeptides at different pH thresholds [25]. Recently, we showed that neuronal AEP is involved in neuronal apoptosis by degrading DNase inhibitor SET during excito-neurotoxicity [26] and that AEP cleaves TDP-43 in post-mortem brain from humans with frontotemporal lobar degeneration [27]. In this report, we show that AEP cleaves tau at both N255 and N368 residues, induces tau aggregation and attenuates its MT stabilizing activity. Furthermore, AEP is highly activated in tau P301S transgenic mice and human AD brains. Consistently, an AEP-cleaved tau fragment at N368 is detected in human AD brains. Knockout of AEP in tau P301S mice leads to the reduction of tau hyperphosphorylation, protecting against memory loss. Blockade of tau cleavage by AEP rescues tau P301S-triggered pathological and behavioral defects. Hence, our results support that tau is a physiological substrate of AEP, and that AEP is a mechanism based therapeutic target for treating tauopathies including AD.

RESULTS

AEP directly cleaves tau

To explore whether AEP proteolytically processes tau, we conducted an *in vitro* cleavage assay with kidney lysates prepared from wild-type (+/+) versus *Lgmn* knockout (–/–) mice under pH 7.4 or 6.0, respectively. Active AEP cleaved tau into two fragments at pH 6.0, whereas inactive AEP at pH 7.4 failed (Fig. 1a, **left panel**). AEP enzymatic activity in kidney lysates was confirmed by the activity assay (Fig. 1a, **right panel**). When cotransfected with GST-tau, wild-type AEP strongly triggered tau fragmentation, while AEP mutants that abolish the cysteine protease activity of AEP (C189S) and the zymogen autocleavage required for its activation (N323A) [25] were unable to provoke tau cleavage, indicating AEP is responsible for eliciting tau proteolytic cleavage (Fig. 1b). Furthermore, the peptide inhibitor AENK completely suppressed tau cleavage by AEP, whereas the inactive control AEQK had no effect (Fig. 1c). The selective anti-AEP antibody also attenuated tau fragmentation (Fig. 1d), suggesting that tau can be specifically cleaved in an AEP-dependent manner. Biochemical assay with purified active AEP and recombinant GST-tau revealed that purified AEP indeed potently and directly cleaved tau (Fig. 1e). Moreover, tau was degraded in both $Lgmn^{+/+}$ and $Lgmn^{+/-}$ mice at pH 6.0, but this effect was substantially attenuated in $Lgmn^{-/-}$ mice. By contrast, at pH 7.4, where AEP is inactive, tau remained intact regardless of AEP genotypes (Fig. 1f). AEP enzymatic activities were also validated by fluorescent substrate cleavage assay (Fig. 1g). Together, these results strongly support that tau is a direct substrate of the cysteine protease AEP.

AEP cleaves endogenous tau at N255 and N368

To identify the cleavage sites on tau by AEP, we purified the fragmented GST-tau proteins with molecular weights of approximately 50 and 60 kDa, respectively, and performed mass spectrometry analysis (Fig. 2a). Two partial-tryptic peptides ending with N255 and N368 for the cleaved recombinant proteins were identified from the LC-MS/MS (Fig. 2b). The amino acid number is based on the longest tau isoform (isoform 2, a.a. 1–441). To avoid unnecessary confusion, we adopted isoform 2's numbering system, though we employed isoform 4 (a.a. 1–352) in all of our *in vitro* experiments. Mutation of either N368A or N255A blocked the appearance of the band at 60kDa or 50kDa, respectively. Tau double

mutant (N255A/N368A) remained completely intact in the presence of active AEP (Fig. 2c), suggesting that N255 and N368 are the two major AEP cleavage sites on tau. Moreover, peptide N368 was identified by MS in human AD brain samples by mass spectrometry (Fig. 2d), supporting that tau cleavage at N368 by AEP occurs in human AD brain. Finally, both N255 and N368 peptides were identified in whole mouse brain extracts and comparative label-free proteomic analysis against *Lgmn*$^{-/-}$ mice revealed greater than 20 folds enrichment for both N368 and N255 in *Lgmn*$^{+/+}$ versus *Lgmn*$^{-/-}$ brain extracts (Fig. 2e). Hence, tau is a physiological substrate of AEP, which cleaves tau at both N255 and N368 sites.

AEP cleaves tau independent of caspases or calpains

Tau can be proteolytically processed by numerous proteinases including caspases, calpains, cathepsins, thrombin, puromycin-sensitive aminopeptidase (PSA) [28]. We assessed the effect of their specific inhibitors on the processing of tau by AEP, and found that tau cleavage was selectively reduced by the specific AEP inhibitor AENK but not by any of the other protease inhibitors (Supplementary Fig. 1a). Remarkably, point mutation of the cleavage sites by various proteases (R155A and K257A for thrombin; M419A for cathepsin; D421E for caspase-3; L43A/V229A for calpain) were prominently fragmented by active AEP, whereas AEP mutant (N255A/N368A) remained intact (Supplementary Fig. 1b). These results indicate that cleavage by other proteases is not necessary for AEP processing of tau. On the other hand, calpain cleavage analysis revealed that tau wild-type, N255A/N368A mutant and tau fragment (1–255) were cleaved in a time-dependent manner with consistent rates (Supplementary Fig. 1c), indicating that AEP cleavage of tau does not affect proteolytic processing by calpains. We made the similar observation with both wild-type and tau N255A/N368A mutant in caspase-3 cleavage assay (Supplementary Fig. 1d). Thus, AEP and other proteases can independently fragment tau. To test whether tau hyperphosphorylation influences tau cleavage by AEP, we pretreated GST-tau transfected HEK293 cells with protein phosphatase PP2 inhibitor okadaic acid (OA), and monitored tau fragmentation. GST-tau was cleaved in a time-dependent manner regardless of OA treatment (Supplementary Fig. 1e,f), indicating that hyperphosphorylation of tau does not interfere with AEP cleavage.

AEP is activated during aging process and in human AD brains

Since age is the major risk factor for AD, and the pH in the brain gradually decreases during aging [29,30], we sought to investigate tau degradation by AEP in the brain at different ages. Tau was fragmented progressively with degradation products detectable as early as 8 months of age (Fig. 3a). To further investigate tau fragmentation by AEP, we developed an anti-tau N368 antibody, which specifically recognized the cleaved tau 1–368 band but not full-length tau or tau 1–255 band (Supplementary Fig. 2a,b). The immunoprecipitated bands by anti-tau N368 antibody was recognized by two different tau antibodies (tau1 and tau5), suggesting indeed AEP-cleaved tau but not other proteins was selectively immunoprecipitated (Supplementary Fig. 2c). We detected tau immunoreactive fragments at 8 and 13 months old mouse brains with anti-tau N368 (Fig. 3a, 2$^{\mathbf{nd}}$ **panel**). In agreement with this finding, we found that AEP activity also increased with aging, correlating with tau cleavage pattern (Fig. 3b). The tau fragmentation was completely abolished in *Lgmn*$^{-/-}$ brain, supporting that tau

degradation during aging is mediated by AEP (Fig. 3c). The anti-tau N368 antibody also robustly labeled tau N368 immunoreactivity in AD brain sections, whereas the signals were markedly attenuated in age-matched control brains (Fig. 3d). Pre-incubation with the antigen peptide (tau 360–368) abolished immunoreactivity (Supplementary Fig. 2d), supporting the specificity of the anti-tau N368 antibody. Furthermore, we found that tau N368 immunoreactive fragments were abundant in human AD brains but barely detectable in controls (Fig. 3e). Moreover, immunofluorescent staining revealed that tau N368 colocalized with thioflavin S-positive NFTs in human AD brains (Fig. 3f), and tau N368 also colocalized with phosphorylated tau (Supplementary Fig. 2e), indicating that AEP induced fragments of tau are constituents of NFTs *in vivo*. AEP enzymatic activities in human AD brains were also higher than controls (Fig. 3g), fitting with the marked tau N368 fragmentation in human AD samples. Further, AEP activity was elevated in tau P301S transgenic mice versus the age-matched control non-transgenic mice (Fig. 3h). As expected, the pH in the transgenic mice brain cortex and hippocampus was decreased compared to non-transgenic control (Fig. 3i). Hence, AEP is activated in aging brain, and it is also activated in both human AD brains and tau P301S transgenic mice.

Noticeably, Aβ oligomers elicited both AEP and tau fragmentation in a dose-dependent manner in primary neuronal cultures (Supplementary Fig. 3a,b). AEP was activated by Aβ dose-dependently, whereas cathepsin B, an AEP-related cysteine protease, was not activated. As expected, caspase-3 activity increased with Aβ in a concentration-dependent manner (Supplementary Fig. 3c–e). Moreover, overexpression of AEP in primary neurons elicited demonstrable tau N368 degradation (Supplementary Fig. 3f). Thus, Aβ may provoke AEP activation, resulting in tau degradation at N368.

AEP cleavage of tau generates neurotoxic fragments

To assess whether AEP cleavage may affect the functions of tau in promoting MT polymerization, we conducted an *in vitro* MT polymerization assay with purified tubulin in the presence of His-tagged tau fragments. As expected, full-length tau strongly augmented MT polymerization; in contrast, the stimulatory effects of truncated tau fragments 1–368 and 256–441 were greatly reduced. Although tau fragment 256–368 moderately increased MT polymerization *in vitro*, tau fragments 1–255 and tau 369–441 failed to induce polymerization (Fig. 4a–c). Accordingly, overexpression of full-length tau in primary neurons notably increased axon length; in contrast, axon elongation was not enhanced in neurons expressing any one of the tau fragments (Fig. 4d).

In neurons transfected with a mixture of the tau fragments, apoptosis was increased more than 60% compared to neurons transfected with full-length tau (Fig. 4e). TUNEL staining showed that the tau truncates, 1–368 and 256–368, triggered substantial apoptosis compared to wild-type or other tau fragments (Fig. 4f). These results were confirmed in neurons infected with adeno-associated virus (AAVs) encoding tau full-length or tau 1–368 (Supplementary Fig. 4a,b). Hence, tau fragments that lack the C-terminal tail after N368 residue cut by AEP are neurotoxic. Furthermore, none of the CDK5, GSK3, and PKA inhibitors (roscovitine, SB216763, and H89, respectively) attenuated the toxic effect of tau

1–368, indicating the neurotoxic effect of tau 1–368 is not dependent on its phosphorylation (Fig. 4g).

AEP-generated tau fragments form insoluble fibrils *in vitro*

To investigate the effect of AEP cleavage on tau fragment propensity for filament formation, we monitored accumulation of PHFs using purified His-tagged tau recombinant proteins. The tau truncate 256–368 displayed the strongest effect on self-assembly into filamentous structures, followed by the tau 1–368 and tau 256–441. These fragments all exhibited a greater ability to form PHFs than full-length tau. Notably, tau 1–255 and tau 369–441 fragments were unable to aggregate into PHFs, whereas the mixture of these aforementioned fragments demonstrated an increased propensity to form PHFs (Supplementary Fig. 5a). Consistent with the Thioflavine S assay, PHFs were observed under negative stain electron microscopy in samples prepared with tau truncates of 1–368, 256–368, 256–441 and full-length tau. Again, a mixture of all of these fragments also formed filamentous structures (Supplementary Fig. 5b). Fractionation of heparin-induced insoluble tau fibrils via ultracentrifugation revealed similar results, with tau fibrils of 256–368, 256–441 and 1–368 displaying the most robust aggregates, followed by full-length tau (Supplementary Fig. 5c). Hence, AEP processing of tau promotes its assembly into filaments.

To explore whether AEP-cleaved tau fragments induce tau phosphorylation, we transfected primary neurons with HA-tagged tau 1–255 or tau 1–368 and performed immunofluorescent staining with anti-AT8. Overexpression of either tau fragment from AEP fragmentation elicited robust AT8 immunoreactivity, whereas full-length tau displayed no signal above endogenous levels (Supplementary Fig. 6). Conceivably, AEP cleaves tau on both N255 and N368 sites, and the resultant fragments elicit tau hyperphosphorylation and aggregation.

Knockout of AEP prevents cognitive deficits in tau P301S mice

To assess the physiological role of AEP in synaptic function and behavior, we bred *Lgmn*$^{-/-}$ mice with tau P301S transgenic mice to knock out AEP in tau P301S mice. The genotypes of transgenic mice were validated (Supplementary Fig. 7). Immunoreactivity for the tau N368 fragment was evident in tau P301S mice, but was not detectable in tau P301S/*Lgmn*$^{-/-}$ mice (Fig. 5a). The absence of tau N368 in tau P301S/*Lgmn*$^{-/-}$ mice was also confirmed by immunohistochemistry (Fig. 5b). Approximately 30% reduction of AT8- and AT100-positive neurons was found in tau P301S/*Lgmn*$^{-/-}$ mice compared to tau P301S transgenic mice both in the hippocampus and cortex (Fig. 5c and Supplementary Fig. 8). Electron microscope analysis of brain sections showed that at 6 months of age, tau P301S mice exhibited overt reduction in synapses compared to wild-type and *Lgmn*$^{-/-}$ mice. Notably, deletion of AEP greatly ameliorated synapse loss in tau P301S mice (Fig. 5d and Supplementary Fig. 9a). Golgi staining revealed that AEP gene deletion prevented the loss of denritic spines in tau P301S mice (Supplementary Fig. 9b,c). Electrophysiological analysis found that the input/output (I/O) relation was suppressed and the averaged field excitatory post-synaptic potentials (fEPSPs) slope was substantially reduced in tau P301S mice compared to wild-type and tau P301S/*Lgmn*$^{-/-}$ mice (Supplementary Fig. 10a,b), indicating that synaptic transmission is impaired in 6 months old tau P301S mice but rescued by AEP gene deletion. The ratios of paired pulse (induced by 100- and 200-ms

intervals) were lower in tau P301S mice but higher in WT and tau P301S mice with AEP knockout (Fig. 5e), suggesting an amelioration of presynaptic dysfunction due to AEP gene deletion. The long-term potentiation (LTP) of fEPSPs in the hippocampal CA1 region, which represents the molecular basis of learning and memory, was also diminished in tau P301S mice compared with the control wild-type and tau P301S/*Lgmn*$^{-/-}$ mice. Hence, knockout of AEP gene in tau P301S mice substantially prevents the impairment in synaptic function caused by the tau mutation (Fig. 5f).

Next, we assessed the effect of deleting *Lgmn* gene on memory functions in tau P301S transgenic mice by the Morris Water Maze. During the training phase, the swim distance and latency to find the platform were progressively decreased, demonstrating a learning effect in the tau P301S transgenic mice, albeit substantially impaired compared to wild-type control or *Lgmn*$^{-/-}$ mice. However, knockout of AEP gene from tau P301S mice greatly reduced the learning deficits (Fig. 5g,h). Probe trail found that deletion of AEP in tau P301S mice improved memory retention as illustrated by the higher percentage of time spent in the target quadrant. All groups of animals displayed comparable swim speed (Fig. 5i), indicating that the genetic manipulations did not have any deleterious effects on motor function.

Next, we also conducted the contextual and cued fear conditioning tests with these animals. Strikingly, tau P301S mice displayed substantially lower levels of freezing compared to the wild-type or *Lgmn*$^{-/-}$ mice. *Lgmn* gene knockout from tau P301S mice increased memory in both the cued fear test and the contextual fear assay (Fig. 5j). Therefore, deletion of AEP greatly reverses the spatial and associative learning deficits in tau P301S transgenic mice.

Preservation of cognition in mice expressing uncleavable tau P301S

To confirm the effects of AEP are mediated via cleavage of tau, we injected AAVs encoding human tau P301S or AEP non-cleavable tau P301S (tau P301SN255AN368A) into the hippocampus of wild-type mice. Two months later, similar levels of tau P301S and tau P301SN255AN368A were detected in the hippocampus by immunohistochemistry and Western blot using the human tau specific antibody HT-7 (Fig. 6a,b). The density of synapse in the hippocampus of mice injected with AAV-tau P301S was substantially less than AAV-GFP control. However, the synaptic density was preserved when the mice were injected with AAV-tau P301SN255AN368A (Fig. 6c,d). Electrophysiological analysis found that the ratios of paired pulse were lower in mice expressing tau P301S compared with mice injected with control virus, indicating evident presynaptic dysfunction. N255AN368A mutation reversed the reduction of paired pulse ratios (Fig. 6e). Notably, the N255AN368A mutation also attenuated the impairment of LTP induced by injection of AAV-tau P301S (Fig. 6f). The slope of I/O curve was suppressed by tau P301S, but not by tau P301SN255AN368A (Fig. 6g,h). These results indicate that the synaptic function is preserved in mice expressing non-cleavable tau P301S. In the Morris Water Maze test, tau P301SN255AN368A mice showed decreased latency to find the platform during the training phase, and increased percentage of time in the target quadrant during the probe test compared to mice injected with AAV-tau P301S, indicating preserved cognitive function (Fig. 6i,j). The preservation of synaptic and cognitive function by the mutation of AEP cleavage site indicates that the cleavage of tau is required for the effects of AEP in the current paradigm.

DISSCUSION

In the present study, we have identified that AEP acts as a physiological protease that cleaves tau in an age-dependent manner in mouse and human brain, including in AD. AEP processes tau at both N255 and N368 sites, inhibiting tau-mediated effects on MT assembly and axon elongation. The resultant C-terminus-deleted tau fragments are prone to aggregate and strongly trigger neurodegeneration, indicating that AEP activation may induce neuronal cell death through proteolytic degradation of tau. These findings fit with the most recent report that AEP is activated in human AD brains, and it translocates from the lysosomes into the cytoplasm [31]. Presumably, the cytoplasmic translocated AEP may cleave tau, leading to disruption of microtubule dynamics, NFT formation, and neurodegeneration. We noticed that the different pathogenic processes are not necessarily associated with the same AEP derived fragment. However, the one AEP derived fragment that does show some of the common toxic effects is tau 1–368. Our data also support that deletion of AEP from tau P301S transgenic mice substantially decreases tau hyperphosphorylation and alleviates synaptic loss and memory deficit in the mice.

Previous studies in a transgenic (tau P301S) tauopathy mouse model revealed that synapse loss and microglial activation precede the appearance of NFTs, presumably due to the impaired transport that results from tau hyperphosphorylation [32]. Here, we provide convergent biochemical and cellular evidence that suggests AEP cleavage of tau also contributes to synaptic loss in tau P301S mice (Fig. 5). Interestingly, tau hyperphosphorylation does not affect tau proteolytic degradation by AEP (Supplementary Fig. 1). Thus, while tau phosphorylation may prevent its cleavage by caspase-3 [33], AEP cleavage of tau appears phosphorylation independent. However, we found that truncation of tau by AEP facilitates tau hyperphosphorylation (Supplementary Fig. 6). Consistent with our findings, the expression of the truncated tau 151–391 in the brain of transgenic animals induces the complete tau cascade of neurofibrillary degeneration as found in humans [34]. Therefore, all these observations strongly support truncation of tau as a key posttranslational modification provoking neurofibrillary degeneration with the pathological features similar to those found in human AD.

AEP levels increase in an age-dependent manner (Fig. 3a). As expected, tau is fragmented by AEP at the age of 8 months, when AEP is augmented. NFTs are the first pathology that occurs during aging and AD and their burden correlates with the degree of cognitive impairment [35–37], providing the initial circumstantial evidence to suggest that toxic gains-of-function by NFTs might play an important part in the progression of the disease. The reduction of hyperphosphorylated tau in tau P301S/*Lgmn*$^{-/-}$ mice compared to age-matched tau P301S mice (Fig. 5) indicates AEP might act as a crucial protease triggering NFT pathology in AD during aging. Moreover, AEP knockout ameliorates synaptic loss, LTP impairment and memory loss in tau P301S transgenic mice, supporting that AEP might be an upstream trigger in AD onset and progression. The preservation of synaptic and cognitive function in mice expressing AEP non-cleavable tau P301S further confirms that the effects of AEP are mediated by the cleavage of tau. Conceivably, blockade of this devastating protease may provide an innovative therapeutic intervention for treating neurodegenerative diseases including AD.

ONLINE METHODS

Mice

Tau P301S mice on a C57BL/6J background (line PS19) and wild-type C57BL/6J mice were products of the Jackson Laboratory (stock number: 008169 and 000664, respectively). The AEP knockout mice on a mixed 129/Ola and C57BL/6 background were generated as reported [38]. Animal care and handling was performed according to the Declaration of Helsinki and Emory Medical School guidelines. Tau P301S mice were crossed with *Lgmn*$^{-/-}$ mice to generate tau P301S/*Lgmn*$^{-/-}$ mice. The following animal groups were analyzed: WT, *Lgmn*$^{-/-}$, tau P301S, tau P301S/*Lgmn*$^{-/-}$. 6-month-old male mice were used for experiments unless otherwise mentioned (8 mice per group). Sample size was determined by Power and Precision (Biostat). Investigators were blinded to the group allocation during the animal experiments. The protocol was reviewed and approved by the Emory Institutional Animal Care and Use Committee.

Human tissue samples

Post-mortem brain samples were dissected from frozen brains of 8 AD cases (age 74.5 ± 11.2 years, mean ± SD) and 8 nondemented controls (age 73.9 ± 12.7 years) from the Emory Alzheimer's Disease Research Center. The study was approved by the Biospecimen Committee. AD was diagnosed according to the criteria of the Consortium to Establish a Registry for AD and the National Institute on Aging. Diagnoses were confirmed by the presence of amyloid plaques and neurofibrillary tangles in formalin-fixed tissue. Informed consent was obtained from the subjects.

Transfection and infection of the cells

HEK293 cells were transfected with plasmids encoding wild-type or point mutant mGST-tau isoform 4 (a.a. 1–352), myc-AEP, myc-AEP C189S, or myc-AEP N323A by the calcium phosphate precipitation method. To express myc-AEP, tau full-length or tau fragments in primary neurons, Lipofectamine 2000 (Invitrogen) was used as described previously [39]. To express tau full-length and tau 1–368 in primary neurons, 1 μl AAV-tau or AAV-tau 1–368 ($1X10^{14}$ vg ml min^{-1}) was added to 1 ml culture medium. The expression of tau full-length and tau 1–368 was assessed 96 h after infection.

In vitro tau cleavage assay

To assess the cleavage of tau by AEP *in vitro*, HEK293 cells were transfected with GST-tau DNA by the calcium phosphate precipitation method. 48 h after transfection, the cells were collected, washed once in PBS, lysed in buffer (50 mM sodium citrate, 5 mM DTT, 0.1% CHAPS and pH 5.5, 0.5% Triton X-100), and centrifuged for 10 min at 14,000 g at 4°C. The supernatant were then incubated with mouse kidney lysate at pH 7.4 or 6.0 at 37°C for 30 min. To test the effect of caspase, cathepsin, calpain, thrombin, PSA and AEP inhibitors on the cleavage of tau by AEP, inhibitors were used against: caspase (ZVAD-fmk, Calbiochem), cathepsin (E64, Sigma-Aldrich), calpains (ALLN, Sigma-Aldrich), thrombin (PMSF, Sigma-Aldrich), PSA (purimycin, Sigma-Aldrich), and AEP (AENK peptide inhibitor and inactive control AEQK). To measure the cleavage of purified tau fragments by

AEP, caspase-3 or calpain, GST-tagged tau full-length or fragments were purified with Glutathione beads. The purified tau protein was incubated with recombinant AEP protein (Novoprotein, 5 μg ml^{-1}) in AEP buffer (50 mM sodium citrate, 5 mM DTT, 0.1% CHAPS, and 0.5% Triton X-100, pH 6.0), recombinant caspase-3 (Calbiochem, 5 ug ml^{-1}) in caspase buffer (100 mM NaCl, 50 mM HEPES, 10 mM DTT, 1 mM EDTA, 10% glycerol, 0.1% CHAPS, pH 7.4), or recombinant calpain (Sigma-Aldrich, 50 ug ml^{-1}) in calpain buffer (50 mM Tris-HCl, 100 mM NaCl, 2 mM DTT, 1mM EDTA, 3 mM $CaCl_2$, pH 7.5). The samples were then boiled in 1XSDS loading buffer and analyzed by immunoblotting.

AEP activity assay and measurement of pH in the brain lysates

Tissue homogenates or cell lysates (10 μg) were incubated in 200 μl assay buffer (20 mM citric acid, 60 mM Na_2HPO_4, 1 mM EDTA, 0.1% CHAPS, and 1 mM DTT, pH 6.0) containing 20 μM AEP substrate Z-Ala-Ala-Asn-AMC (Bachem). AMC released by substrate cleavage was quantified by measuring at 460 nm in a fluorescence plate reader at 37°C for 1 h in kinetic mode for 5 min. The pH of hippocampus and cortex of tau P301S and control mice was read at 37°C using 2% (wt/vol) brain homogenates in distilled water as described previously [29].

Mass spectrometry analysis

Protein samples were in-gel digested with trypsin. Peptide samples were resuspended in loading buffer (0.1% formic acid, 0.03% trifluoroacetic acid, 1% acetonitrile) and loaded onto a 20 cm nano-HPLC column (internal diameter 100 μm) packed with Reprosil-Pur 120 C18-AQ 1.9 μm beads (Dr. Maisch) and eluted over a 2 h 4–80% buffer B reverse phase gradient (Buffer A: 0.1% formic acid, 1% acetonitrile in water; Buffer B: 0.1% formic acid in acetonitrile) generated by a NanoAcquity UPLC system (Waters Corporation). Peptides were ionized with 2.0 kV electrospray ionization voltage from a nano-ESI source (Thermo) on a hybrid LTQ XL Orbitrap mass spectrometer (Thermo). Data dependent acquisition of centroid MS spectra at 30,000 resolution and MS/MS spectra were obtained in the LTQ following collision induced dissociation (collision energy 35%, activation Q 0.25, activation time 30 ms) for the top 10 precursor ions with charge determined by the acquisition software to be $z \geq 2$. Dynamic exclusion of peaks already sequenced was for 20 s with early expiration for 2 count events with signal-to-noise > 2. Automatic gating control was set to 150 ms maximum injection time or 10^6 counts. To identify AEP cleavage sites on human tau, the SageN Sorcerer SEQUEST 3.5 algorithm was used to search and match MS/MS spectra to a complete semi-tryptic human proteome database (NCBI reference sequence revision 50, with 66,652 entries) plus pseudo-reversed decoys sequences [40,41] with a 20 ppm mass accuracy threshold. Only b and y ions were considered for scoring (Xcorr) and Xcorr along with ΔCn were dynamically increased for groups of peptides organized by a combination of trypticity (fully or partial) and precursor ion charge state to remove false positive hits along with decoys until achieving a false discovery rate (FDR) of < 5% (< 0.25% for proteins identified by more than one peptide). The FDR was estimated by the number of decoy matches (nd) and total number of assigned matches (nt). FDR = 2*nd/nt, assuming mismatches in the original database were the same as in the decoy database. All semi-tryptic MS/MS spectra for putative AEP generated APP cleavage sites were manually

inspected. A user defined precursor mass tolerance of ± 20 ppm was employed for extracted ion chromatogram (XIC) based quantification as previously described [42].

Western blot analysis

The mouse brain tissue or human tissue samples was lysed in lysis buffer (50 mM Tris, pH 7.4, 40 mM NaCl, 1 mM EDTA, 0.5% Triton X-100, 1.5 mM Na_3VO_4, 50 mM NaF, 10 mM sodium pyrophosphate, 10 mM sodium β-glycerophosphate, supplemented with protease inhibitors cocktail), and centrifuged for 15 min at 16,000 g. The supernatant was boiled in SDS loading buffer. After SDS-PAGE, the samples were transferred to a nitrocellulose membrane. Primary antibodies to the following targets were used: GST-HRP (Sigma-Aldrich), tubulin (Sigma-Aldrich), HA and myc (both from Santa Cruz), His (GE healthcare), HT7, tau5, AT8 and AT100 (Thermo), and tau-1 (Calbiochem).

Immunostaining

For visualization of PHF-tau, Free-floating 30 μm brain sections the brain sections were treated with 0.3% H_2O_2 for 10 min. Then, sections were washed three times in PBS and blocked in 1% BSA, 0.3% Triton X-100, for 30 min followed by overnight incubation with anti-tau N368, anti-AT8 or anti-AT100 antibody (1: 500) at 4°C. The signal was developed using Histostain-SP kit (Invitrogen). To detect the localization of AEP-cleaved tau and PHF in human AD brain sections, the sections were incubated with mouse anti-tau N368 primary antibody overnight at 4°C. The sections were washed three times in PBS, and incubated with Texas Red conjugated anti-mouse IgG for 1 h at room temperature. After brief rinse in PBS, the sections were stained for 5 min with 0.0125% Thioflavin-S in 50% ethanol. The sections were washed with 50% ethanol and placed in distilled water. Then the sections were covered with a glass cover using mounting solution and examined under a fluorescence microscope.

Purification of recombinant tau protein and preparation of PHF

His-tagged full-length tau, tau 1–255, 1–368, 256–368, 256–441, and 368–441 was purified from *E. coli* using His bind purification kit (Calbiochem). The purified tau fragments were induced to aggregate as described previously [43]. Briefly, purified tau fragments (50 μM) were incubated in PBS (pH 7.4) containing 12.5 μM heparin, 2 mM DTT and a protease inhibitor cocktail. The samples were incubated with 50 μM thioflavin S for 45 min in the dark at room temperature. PHF formation was quantified by measuring the fluorescence with an excitation at 440 nm and an emission wavelength of 510 nm. The overall appearance of the PHFs was visualized by negative stain electron microscopy. Briefly, the reaction samples was adsorbed onto carbon/formvar-coated 400 mesh copper grids (EM Sciences) for 30 s, and stained with 2% uranyl acetate for 30 s. Excess liquid in the sample was wicked using filter paper. The grids were examined with a Philips 208S electron microscope (Philips, Hillsboro, OR). The remaining solutions of aggregated tau were centrifuged at 100,000 g for 30 min to separate aggregated tau pallet and non-aggregated tau supernatant, and analyzed by Western blot.

Microtubule assembly assay

His-tagged full-length tau and tau fragments were purified from *E. coli.* 1.5 μM tau fragments were incubated with 20 μM tubulin (Cytoskeleton) at 37°C, and polymerization of microtubules was monitored by measuring the absorbance at 350 nm over 20 min as described previously [44].

AAV vector packaging

pAAV vectors carrying the longest human tau isoform (Tau4R2N) or GFP use the human synapsin I promoter to drive neuron-specific gene expression [45]. All of the mutations were introduced using site-directed mutagenesis kit (Agilent Technologies). The AAV particles were prepared by Viral Vector Core at Emory University.

Stereotaxic injection of the virus

3-month-old wild-type C57BL/6J mice were anesthetized with phenobarbital (75 mg kg^{-1}). Bilateral intracerebral injection of AAV-GFP, AAV-tau P301S, and AAV-tau P301SN255AN368A was performed stereotactically at coordinates posterior 1.94 mm, lateral 1.4 mm, ventral 2.2 mm relative to bregma. 2 μl of viral suspension containing $2X10^{11}$ vector genome (vg) was injected in to each point using 10 μl glass syringes with a fixed needle at a rate of 0.5 μl min^{-1}. The needle was remained in place for 5 min before it was removed slowly (throughout 2 min). The mice were placed on heating pad until it began to recover from the surgery.

Electron microscopy of synapse

Synaptic density was determined by electron microscopy. Briefly, after deep anesthesia, mice were perfused transcardially with 2% glutaraldehyde and 3% paraformaldehyde in PBS. Hippocampal slices were postfixed in cold 1% OsO_4 for 1 h. Samples were prepared and examined using standard procedures. Ultrathin sections (90 nm) were stained with uranyl acetate and lead acetate and viewed at 100 kV in a JEOL 200CX electron microscope. Synapses were identified by the presence of synaptic vesicles and postsynaptic densities. Synapse density in area CA1 of the hippocampus was calculated.

Golgi stain

Mouse brains were fixed in 10% formalin for 24 h, and then immersed in 3% potassium bichromate for 3 d in the dark. The solution was changed each day. Then the brains were transferred into 2% silver nitrate solution and incubated for 24 h in the dark. Vibratome sections were cut at 60 μm, air dried for 10 min, dehydrated through 95% and 100% ethanol, cleared in xylene and assembled on coverslips. Bright-field images of pyramidal neurons in the hippocampus and cortex were taken at 100X magnification using a Zeiss Axioplan (Zeiss, Decatur, GA, USA) microscope. To measure the spine density, all clearly evaluable areas of 50–100 μm of secondary dendrites from each imaged neuron were used.

Electrophysiology

Acute hippocampal transversal slices were prepared form 6-month-old WT, *Lgmn*$^{-/-}$, tau P301S, tau P301S/*Lgmn*$^{-/-}$ mice as previously described [44]. Briefly, mice hippocampi were

dissected and cut into 400-μm thick transverse slices. A 0.1 M tungsten monopolar electrode was used to stimulate the Schaffer collaterals. The field excitatory post-synaptic potentials (fEPSPs) were recorded in CA1 stratum radiatum by a glass microelectrode filled with artificial CSF with resistance of 3–4 MΩ. Field potential input-output curves were constructed by measuring fEPSP slopes responding to the stimulus intensity increasing from 0.5 to 10 V, with an 0.5 V increment. Paired-pulse facilitation (PPF) was examined by applying pairs of pulses which were separated by 20–500 ms intervals. LTP of fEPSPs was induced by 3 theta-burst-stimulation (TBS); it is 4 pulses at 100 Hz, repeated 3 times with a 200-ms interval). The magnitudes of LTP are expressed as the mean percentage of baseline fEPSP initial slope.

Generation of antibodies that specifically recognize the AEP-generated tau fragment (anti-tau N368)

Three Balb/c mice were immunized with the peptide Ac-CITHVPGGGN-OH that includes the 9 amino acids in tau that precede the AEP cleavage site at N368 as well as an amino-terminal cysteine residue to allow coupling to KLH. The mice were boosted 4 times with the immunizing peptide with 3-week intervals between injections. The antiserum was pooled and the titers against the immunizing peptide were determined by ELISA. The maximal dilution giving a positive response using chromogenic substrate for horseradish peroxidase was 1: 30000. The immunoactivity of the antiserum was further confirmed by Western blot and immunohistochemistry.

Morris water maze

6-month-old WT, *Lgmn*$^{-/-}$, tau P301S, tau P301S/*Lgmn*$^{-/-}$ mice were trained in a round, water-filled tub (52 inch diameter) in an environment rich with extra maze cues as described previously [44]. Each subject was given 4 trials/day for 5 consecutive days with a 15-min inter-trial interval. The maximum trial length was 60 s and if subjects did not reach the platform in the allotted time, they were manually guided to it. Following the 5 d of task acquisition, a probe trial was presented during which time the platform was removed and the percentage of time spent in the quadrant which previously contained the escape platform during task acquisition was measured over 60 s. All trials were analysed for latency and swim speed by means of MazeScan (Clever Sys, Inc.).

Fear conditioning test

The ability to form and retain an association between an aversive experience and environmental cues was tested with a standard fear conditioning paradigm that occurs over a period of three days. Mice were placed in the fear conditioning apparatus (7″ W, 7″ D X 12″ H, Coulbourn) composed of plexiglass with a metal shock grid floor and allowed to explore the enclosure for 3 min. Following this habituation period, 3 conditioned stimulus (CS)-unconditioned stimulus (US) pairings was presented with a 1 min intertrial interval. The CS was composed of a 20 second 85 db tone and US was composed of 2 s of a 0.5 mA footshock, which was co-terminate with each CS presentation. One minute following the last CS-US presentation, mice were returned to their home cage. On day 2 the mice were presented with a context test, during which subjects were placed in the same chamber used

during conditioning on Day 1, and the amount of freezing was recorded via a camera and the software provided by Colbourn. No shocks were given during the context test. On day 3, a tone test was presented, during which time subjects were exposed to the CS in a novel compartment. Initially, animals were allowed to explore the novel context for 2 min. Then the 85 db tone was presented for 6-min, and the amount of freezing behaviour was recorded.

Primary neuron cultures

Primary rat cortical neurons were cultured as previously described [26]. To measure the effect of tau fragments on neurons, neurons cultured 7 days *in vitro* (DIV 7) were transfected with myc-AEP, HA-tau full-length, or HA-tau fragments using Lipofectamine 2000 (Invitrogen). 72 h later, the neurons were fixed in 4% formaldehyde, permeabilized and immunostained with anti-MAP2, anti-myc, anti-HA, anti-AT8, anti-AT100, or anti-tau N368 antibody. The toxic effect of tau fragments was detected with the *In situ* cell death detection kit (Roche). The apoptotic index was expressed as the percentage of TUNEL-positive neurons out of the total number of MAP2-positive neurons.

Caspase and cathepsin activity assay

Cell lysates (10 μg) were incubated in 200 μl caspase assay buffer (100 mM HEPES 0.1% CHAPS, 10% sucrose, pH 7.4) containing 25 μM caspase substrate Ac-Asp-Glu-Val-Asp-AMC (Bachem), or in 200 μl cathepsin assay buffer (100 mM sodium acetate, 1 mM EDTA, pH 5.5) containing 25 μM cathepsin substrate *D*-Val-Leu-Lys-AMC (Bachem) for 1 h. AMC released by substrate cleavage was quantified by measuring at 460 nm in a fluorescence plate reader.

Statistical analysis

Statistical analysis were performed using either Student's t-test (two-group comparison) or one-way ANOVA followed by LSD post hoc test (more than two groups), and differences with *P* values less than 0.05 were considered significant.

Supplementary Material

Refer to Web version on PubMed Central for supplementary material.

Acknowledgments

This work was supported by grants from RO1 (NS045627 and NS060680) from NIH to K. Y., the NIH/NIAP50 ADRC center grant to A.I.L., grant from National Natural Science Foundation of China (No. 81100958) to Z. Z., National Key Basic Research Program of China Grant (2010CB945202) to Y.E.S and National Science Foundation of China Grant (81330030) to L.C. and Y.E.S. We thank D. Weinshenker (Emory University) for tau P301S transgenic mice, S. Kuegler (Max Planck Institute of Psychiatry, Germany) for pAAV vectors carrying tau GFP, and C. Hales (Emory University) for technical support.

References

1. Ballatore C, Lee VM, Trojanowski JQ. Tau-mediated neurodegeneration in Alzheimer's disease and related disorders. Nat Rev Neurosci. 2007; 8:663–672. [PubMed: 17684513]
2. Binder LI, Frankfurter A, Rebhun LI. The distribution of tau in the mammalian central nervous system. J Cell Biol. 2565; 101:1371–1378. [PubMed: 3930508]

3. Harada A, et al. Altered microtubule organization in small-calibre axons of mice lacking tau protein. Nature. 1994; 369:488–491. [PubMed: 8202139]
4. Esmaeli-Azad B, McCarty JH, Feinstein SC. Sense and antisense transfection analysis of tau function: tau influences net microtubule assembly, neurite outgrowth and neuritic stability. J Cell Sci. 1994; 107 (Pt 4):869–879. [PubMed: 8056843]
5. Caceres A, Kosik KS. Inhibition of neurite polarity by tau antisense oligonucleotides in primary cerebellar neurons. Nature. 1990; 343:461–463. [PubMed: 2105469]
6. Dixit R, Ross JL, Goldman YE, Holzbaur EL. Differential regulation of dynein and kinesin motor proteins by tau. Science. 2008; 319:1086–1089. [PubMed: 18202255]
7. Lindwall G, Cole RD. Phosphorylation affects the ability of tau protein to promote microtubule assembly. J Biol Chem. 2564; 259:5301–5305. [PubMed: 6425287]
8. Iqbal K, Zaidi T, Bancher C, Grundke-Iqbal I. Alzheimer paired helical filaments. Restoration of the biological activity by dephosphorylation. FEBS Lett. 1994; 349:104–108. [PubMed: 8045285]
9. Kopke E, et al. Microtubule-associated protein tau. Abnormal phosphorylation of a non-paired helical filament pool in Alzheimer disease. J Biol Chem. 1993; 268:24374–24384. [PubMed: 8226987]
10. Alonso AC, Grundke-Iqbal I, Iqbal K. Alzheimer's disease hyperphosphorylated tau sequesters normal tau into tangles of filaments and disassembles microtubules. Nat Med. 1996; 2:783–787. [PubMed: 8673924]
11. Alonso AC, Zaidi T, Grundke-Iqbal I, Iqbal K. Role of abnormally phosphorylated tau in the breakdown of microtubules in Alzheimer disease. Proc Natl Acad Sci USA. 1994; 91:5562–5566. [PubMed: 8202528]
12. Alonso A, Zaidi T, Novak M, Grundke-Iqbal I, Iqbal K. Hyperphosphorylation induces self-assembly of tau into tangles of paired helical filaments/straight filaments. Proc Natl Acad Sci USA. 2001; 98:6923–6928. [PubMed: 11381127]
13. Gamblin TC, et al. Caspase cleavage of tau: linking amyloid and neurofibrillary tangles in Alzheimer's disease. Proc Natl Acad Sci USA. 2003; 100:10032–10037. [PubMed: 12888622]
14. Rissman RA, et al. Caspase-cleavage of tau is an early event in Alzheimer disease tangle pathology. J Clin Invest. 2004; 114:121–130. [PubMed: 15232619]
15. Basurto-Islas G, et al. Accumulation of aspartic acid421- and glutamic acid391-cleaved tau in neurofibrillary tangles correlates with progression in Alzheimer disease. J Neuropathol Exp Neurol. 2008; 67:470–483. [PubMed: 18431250]
16. Saito K, Elce JS, Hamos JE, Nixon RA. Widespread activation of calcium-activated neutral proteinase (calpain) in the brain in Alzheimer disease: a potential molecular basis for neuronal degeneration. Proc Natl Acad Sci USA. 1993; 90:2628–2632. [PubMed: 8464868]
17. Park SY, Ferreira A. The generation of a 17 kDa neurotoxic fragment: an alternative mechanism by which tau mediates beta-amyloid-induced neurodegeneration. J Neurosci. 2005; 25:5365–5375. [PubMed: 15930385]
18. Arai T, Guo JP, McGeer PL. Proteolysis of non-phosphorylated and phosphorylated tau by thrombin. J Biol Chem. 2005; 369:5145–5153. [PubMed: 15542598]
19. Yang AJ, Chandswangbhuvana D, Margol L, Glabe CG. Loss of endosomal/lysosomal membrane impermeability is an early event in amyloid Abeta1–42 pathogenesis. J Neurosci Res. 1998; 52:691–698. [PubMed: 9669318]
20. Kenessey A, Nacharaju P, Ko LW, Yen SH. Degradation of tau by lysosomal enzyme cathepsin D: implication for Alzheimer neurofibrillary degeneration. J Neurochem. 1997; 69:2026–2038. [PubMed: 9349548]
21. Johnson GV, et al. The tau protein in human cerebrospinal fluid in Alzheimer's disease consists of proteolytically derived fragments. J Neurochem. 1997; 68:430–433. [PubMed: 8978756]
22. Portelius E, et al. Characterization of tau in cerebrospinal fluid using mass spectrometry. J Proteome Res. 2008; 7:2114–2120. [PubMed: 18351740]
23. Chen JM, Dando PM, Stevens RA, Fortunato M, Barrett AJ. Cloning and expression of mouse legumain, a lysosomal endopeptidase. Biochem J. 1998; 335 (Pt 1):111–117. [PubMed: 9742219]

24. Chen JM, Rawlings ND, Stevens RA, Barrett AJ. Identification of the active site of legumain links it to caspases, clostripain and gingipains in a new clan of cysteine endopeptidases. FEBS Lett. 1998; 441:361–365. [PubMed: 9891971]
25. Li DN, Matthews SP, Antoniou AN, Mazzeo D, Watts C. Multistep autoactivation of asparaginyl endopeptidase *in vitro* and *in vivo*. J Biol Chem. 2003; 278:38980–38990. [PubMed: 12860980]
26. Liu Z, et al. Neuroprotective actions of PIKE-L by inhibition of SET proteolytic degradation by asparagine endopeptidase. Mol Cell. 2008; 29:665–678. [PubMed: 18374643]
27. Herskowitz JH, et al. Asparaginyl endopeptidase cleaves TDP-43 in brain. Proteomics. 2012; 12:2455–2463. [PubMed: 22718532]
28. Wang Y, Garg S, Mandelkow EM, Mandelkow E. Proteolytic processing of tau. Biochem Soc Trans. 2010; 38:955–961. [PubMed: 20658984]
29. Yates CM, Butterworth J, Tennant MC, Gordon A. Enzyme activities in relation to pH and lactate in postmortem brain in Alzheimer-type and other dementias. J Neurochem. 1990; 55:1624–1630. [PubMed: 2213015]
30. Pirchl M, Humpel C. Does acidosis in brain play a role in Alzheimer's disease? Neuropsychiatr. 2009; 23:187–192. [PubMed: 19703385]
31. Basurto-Islas G, Grundke-Iqbal I, Tung YC, Liu F, Iqbal K. Activation of asparaginyl endopeptidase leads to tau hyperphosphorylation in Alzheimer disease. J Biol Chem. 2013; 288:17495–17507. [PubMed: 23640887]
32. Yoshiyama Y, et al. Synapse loss and microglial activation precede tangles in a P301S tauopathy mouse model. Neuron. 2007; 53:337–351. [PubMed: 17270732]
33. Guillozet-Bongaarts AL, et al. Pseudophosphorylation of tau at serine 422 inhibits caspase cleavage: *in vitro* evidence and implications for tangle formation *in vivo*. J Neurochem. 2006; 97:1005–1014. [PubMed: 16606369]
34. Zilka N, et al. Truncated tau from sporadic Alzheimer's disease suffices to drive neurofibrillary degeneration *in vivo*. FEBS Lett. 2006; 580:3582–3588. [PubMed: 16753151]
35. Arriagada PV, Growdon JH, Hedley-Whyte ET, Hyman BT. Neurofibrillary tangles but not senile plaques parallel duration and severity of Alzheimer's disease. Neurology. 1992; 42:631–639. [PubMed: 1549228]
36. Arriagada PV, Marzloff K, Hyman BT. Distribution of Alzheimer-type pathologic changes in nondemented elderly individuals matches the pattern in Alzheimer's disease. Neurology. 1992; 42:1681–1688. [PubMed: 1307688]
37. Braak H, Braak E. Staging of Alzheimer's disease-related neurofibrillary changes. Neurobiol Aging. 1995; 16:271–278. discussion 278–284. [PubMed: 7566337]
38. Shirahama-Noda K, et al. Biosynthetic processing of cathepsins and lysosomal degradation are abolished in asparaginyl endopeptidase-deficient mice. J Biol Chem. 2003; 278:33194–33199. [PubMed: 12775715]
39. Kaech S, Banker G. Culturing hippocampal neurons. Nat Protoc. 2006; 1:2406–2415. [PubMed: 17406484]
40. Elias JE, Gygi SP. Target-decoy search strategy for increased confidence in large-scale protein identifications by mass spectrometry. Nat Methods. 2007; 4:207–214. [PubMed: 17327847]
41. Xu P, Duong DM, Peng J. Systematical Optimization of Reverse-Phase Chromatography for Shotgun Proteomics. J Proteome Res. 2009; 8:3944–3950. [PubMed: 19566079]
42. Herskowitz JH, et al. Phosphoproteomic analysis reveals site-specific changes in GFAP and NDRG2 phosphorylation in frontotemporal lobar degeneration. J Proteome Res. 2010; 9:6368–6379. [PubMed: 20886841]
43. Barghorn S, Biernat J, Mandelkow E. Purification of recombinant tau protein and preparation of Alzheimer-paired helical filaments *in vitro*. Methods Mol Biol. 2005; 299:35–51. [PubMed: 15980594]
44. Hong Y, et al. SRPK2 phosphorylates tau and mediates the cognitive defects in Alzheimer's disease. J Neurosci. 2012; 32:17262–17272. [PubMed: 23197718]
45. Jaworski T, et al. AAV-tau mediates pyramidal neurodegeneration by cell-cycle re-entry without neurofibrillary tangle formation in wild-type mice. PLoS One. 2009; 4:e7280. [PubMed: 19794916]

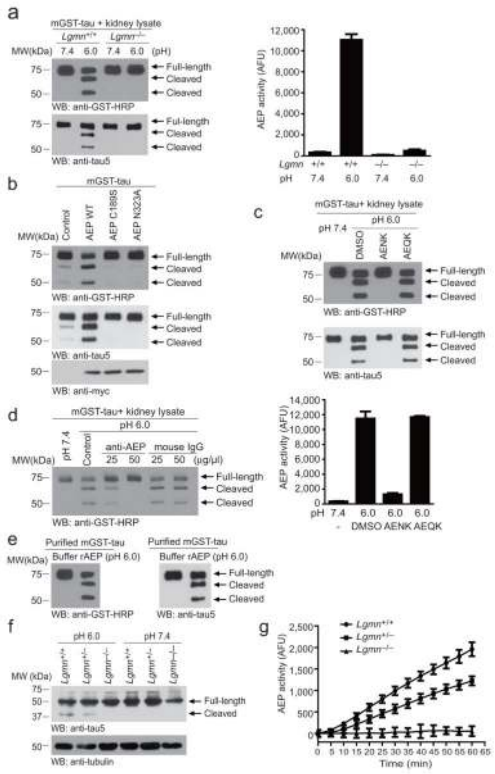

Figure 1. AEP cleaves tau *in vitro*

(**a**) Tau cleavage assay. GST-tau was incubated with kidney lysates from *Lgmn*$^{+/+}$ or *Lgmn*$^{-/-}$ mice at pH 7.4 or pH 6.0 at 37°C for 30 min. Western blot shows that tau was cleaved at pH 6.0 by *Lgmn*$^{+/+}$ kidney lysates (left panel) when AEP was activated (right panel) (mean ± SEM; *n* =3). (**b**) Tau cleavage by wild-type and mutant AEP. HEK293 cells cotransfected with GST-tau and myc-AEP WT, myc-AEP C189S, myc-AEP N323A or control plasmid were incubated in buffer (pH 6.0) at 37°C for 30 min. Tau was selectively cleaved in cells expressing wild-type but not mutant AEP. (**c**) The proteolysis of tau is blocked by AENK peptide, but not AEQK (upper panel). AEP activity was inhibited by AENK (bottom panel) (mean ± SEM; *n* =3). (**d**) Antibody titration assay. AEP specific antibody inhibited the cleavage of tau. Mouse IgG was used as negative control. (**e**) Purified active recombinant AEP potently cleaves purified GST-tau recombinant protein. (**f**) Endogenous tau cleavage by AEP. *Lgmn*$^{+/+}$, *Lgmn*$^{+/-}$, and *Lgmn*$^{-/-}$ mouse brain tissues were lysed in buffer at pH 6.0 or 7.4 and subjected to Western blot. (**g**) Validation of AEP enzymatic activities by fluorescent substrate cleavage assay (mean ± SEM; *n* =3).

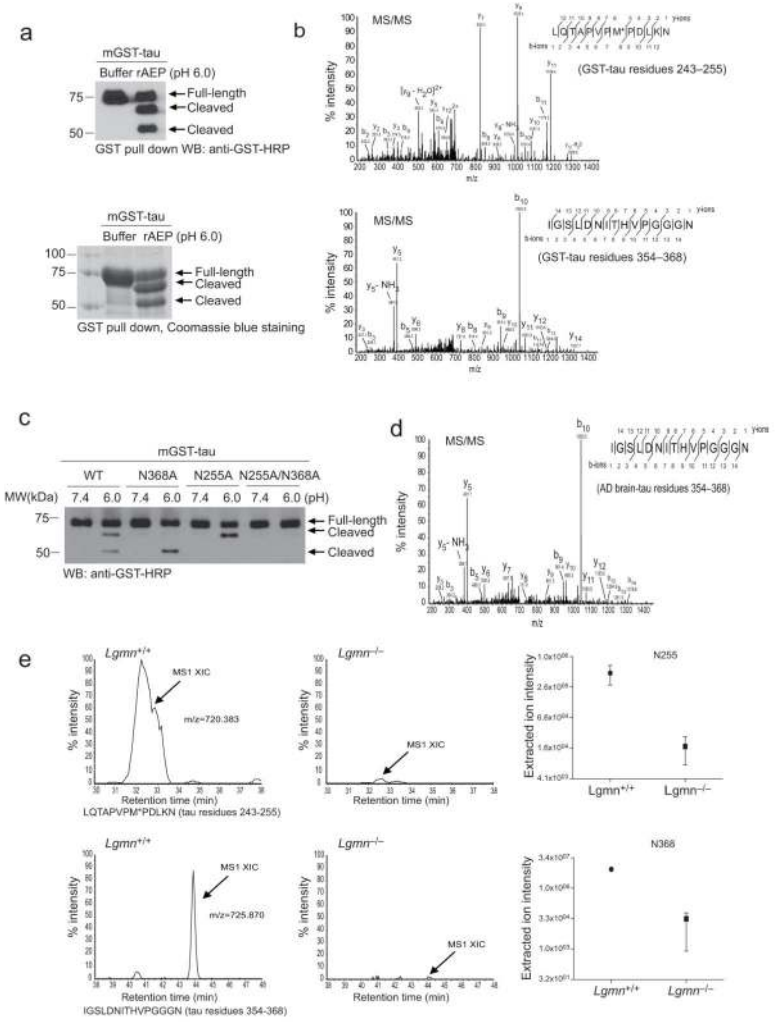

Figure 2. AEP cleaves tau at N255 and N368 residues

(**a**) Cleavage of purified GST-tau analyzed by immunoblotting (upper panel) or Coomassie blue staining (bottom panel). (**b**) Mass spectrometry analysis of recombinant tau fragmented by AEP. The detected MS/MS peptide spectra are listed. (**c**) Cleavage of mutant tau by AEP. Tau cleavage was analyzed by Western blot after GST-tau wide-type, N255A, N368A, or N255A/N368A mutant were incubated with active mouse kidney lysates. (**d**) MS/MS spectrum showing the cleavage of tau after N368 in brain samples from subjects with AD. (**e**) Representative extracted ion chromatograms for tau N255 and N368 peptide from wild-type and *Lgmn*$^{-/-}$ mouse brain samples. Signal intensities were then normalized to wild-type samples, setting the maximum signal intensity to 100%. Values are represented as raw peptide extracted ion intensity.

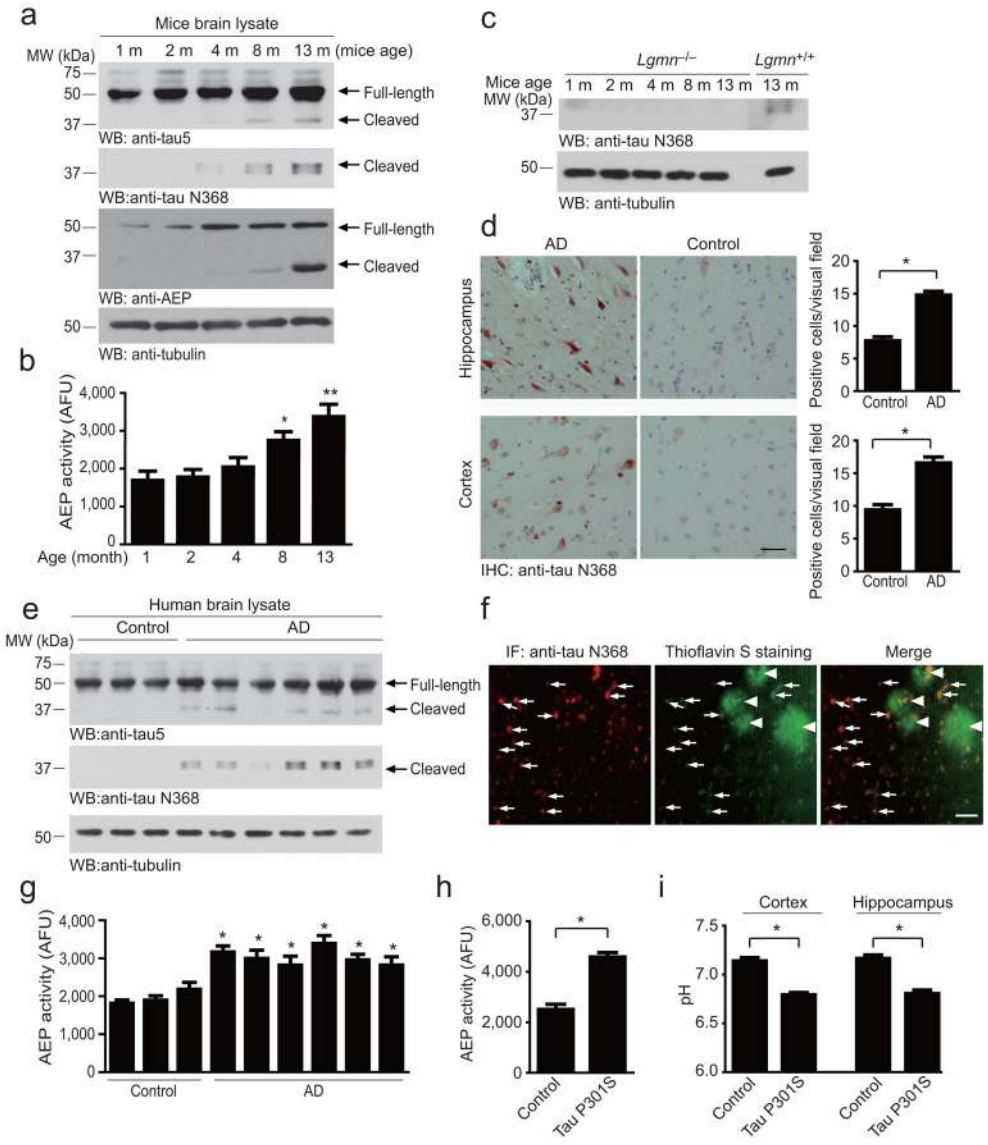

Figure 3. AEP is upregulated and cleaves tau during aging and in Alzheimer's disease

(**a**) Western blot analysis of tau and AEP in mouse brain during aging process. (**b**) AEP activity assay (mean ± SEM; $n = 6$; *$P < 0.05$ compared with 1- and 2-months old mouse brain, **$P < 0.01$ compared with 1-, 2-, and 4-months old mouse brain, one-way ANOVA). (**c**) Western blot detection of tau fragments in the $Lgmn^{-/-}$ and $Lgmn^{+/+}$ mice brain. (**d**) Immunostaining of tau N368 fragments in brain sections of subjects with AD (mean ± SEM, *$P < 0.01$, Student's t-test). Scale bar, 50 μm. (**e**) Western blot detection of tau fragments in human brain samples from subjects with AD and age-matched controls. (**f**) Immunostaining showing colocalization of tau N368 fragment with PHFs. Brain sections from subjects with AD were immunostained with anti-tau N368 antibody, and then stained with Thioflavin S, which labels both the senile plaque (arrow head) and PHFs (arrow). Scale bar, 50 μm. (**g**) AEP activity assay in brain samples from subjects with AD and age-matched controls (mean ± SEM; *$P < 0.05$ compared with control group, one-way ANOVA). (**h**) AEP activity assay in 6-month-old tau P301S mice and non-transgenic controls (mean ± SEM; $n = 6$; *$P < 0.01$,

Student's t-test). (**i**) pH in the brain cortex and hippocampus of control and tau P301S transgenic mice ($n = 6$, $^*P < 0.01$, Student's t-test).

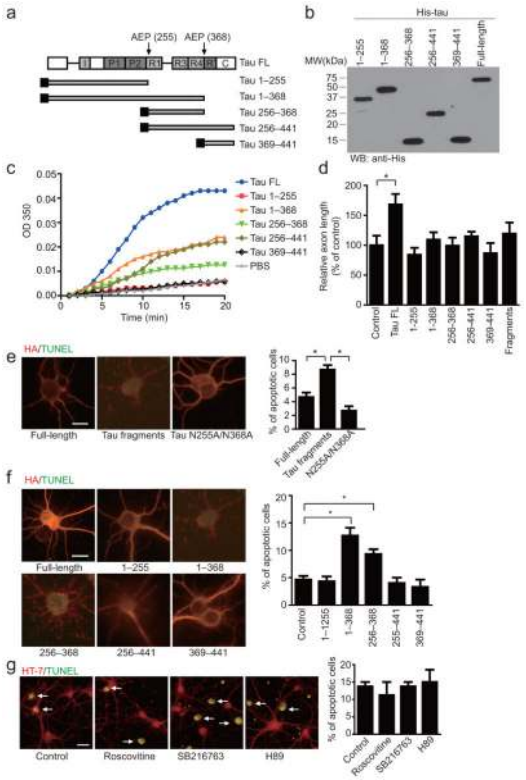

Figure 4. Tau cleavage by AEP disrupts its microtubule assembly activity and is toxic to neurons

(**a**) Schematic diagram of tau isoform 4 domains and its cleavage by AEP. I, Inserts; P, proline rich; R, repeats; R′, pseudo-repeat; C, C-terminal tail. (**b**) Western blot analysis of purified His-tagged tau fragments. (**c**) Microtubule assembly assay. (**d**)Axon elongation in primary neurons transfected with control plasmid, HA-tau, or HA-tau fragments (mean ± SEM; $n = 5$; $^*P < 0.05$, one-way ANOVA). (**e, f**) TUNEL assay showing the neurotoxicity of AEP-derived tau fragments. Mixed tau fragments (**e**), tau 1–368 and tau 256–368 (**f**) induced significant neuronal apoptosis (mean ± SEM; $n = 3$; $^*P < 0.01$, one-way ANOV). Scale bar, 10 μm. (**g**) Effect of kinase inhibitors on the neurotoxic effect of tau 1–368. Primary neurons infected with AAV-tau 1–368 were treated with 10 μM roscovitine (CDK5 inhibitor), SB216763 (GSK3 inhibitor), or H89 (PKA inhibitor) for 12 h. Cell apoptosis was detected by TUNEL staining ($n = 4$). Scale bar, 20 μm.

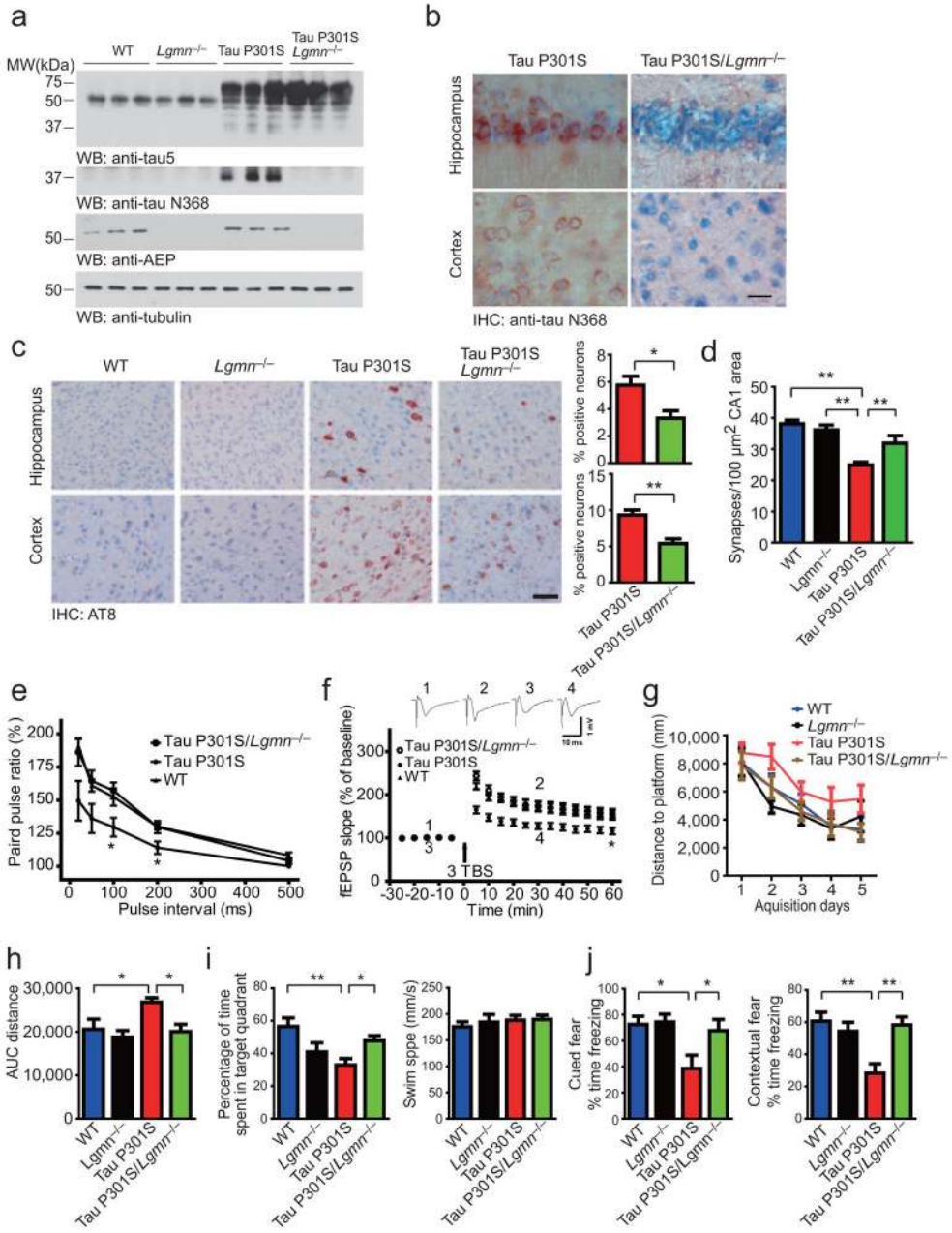

Figure 5. AEP gene deficiency prevents tau phosphorylation, synaptic dysfunction, and memory deficits in the tau P301S mouse

(**a**) The processing of tau in WT, *Lgmn*$^{-/-}$, tau P301S, and tau P301S/*Lgmn*$^{-/-}$ mice. (**b**) Immunostaining of AEP-derived tau fragments in brain sections of tau P301S and tau P301S/*Lgmn*$^{-/-}$ mice. Scale bar, 20 µm. (**c**) AT8 immunostaining of hippocampal and cortex neurons (mean ± SEM; **P* < 0.05, ***P* < 0.01, Student's t-test). Scale bar, 50 µm. (**d**) Synaptic density analysis (mean ± SEM; *n* = 6; ***P* < 0.01, one-way ANOVA). (**e**) The ratio of paired pulses (mean ± SD; *n* = 6 in each group; **P* < 0.05, one-way ANOVA). (**f**) LTP of fEPSPs (mean ± SD; *n* = 6 in each group; **P* < 0.05, one-way ANOVA). Shown traces are representative fEPSPs recorded at the time point 1 and 2 (tau P301S/*Lgmn*$^{-/-}$), 3 and 4 (tau

P301S). (**g, h**) Morris water maze analysis as distance traveled (millimeters) and integrated distance (AUC) for WT, *Lgmn*$^{-/-}$, tau P301S and tau P301S/*Lgmn*$^{-/-}$ mice (mean ± SEM; $n = 8$; $^{*}P < 0.05$, one-way ANOVA). (**i**) Probe trail of Morris water maze test (left panel, mean ± SEM; $n = 8$; $^{*}P < 0.05$, $^{**}P < 0.01$, one-way ANOVA). AEP gene deletion did not interfere with the swim speed (right panel, mean ± SEM; $n = 8$; $P = 0.786$, one-way ANOVA). (**j**) Fear conditioning test. Tau P301S/*Lgmn*$^{-/-}$ mice show more freezing time than tau P301S littermates both in cued fear conditioning test (left panel), and contextual fear conditioning test (right panel) (mean ± SEM; $n = 8$; $^{*}P < 0.05$, $^{**}P < 0.01$, one-way ANOVA).

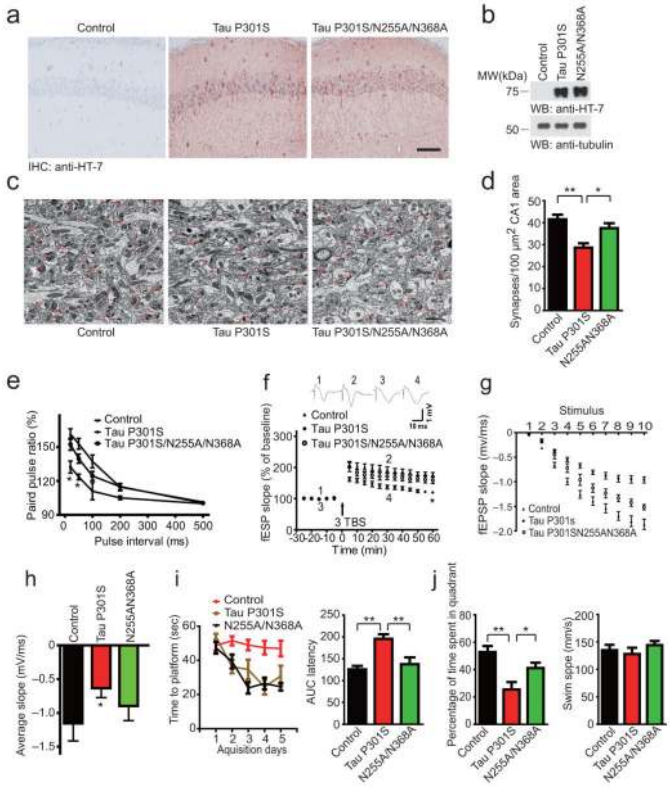

Figure 6. Blocking of tau cleavage by AEP prevents tau P301S-induced synaptic dysfunction and cognitive impairment

(**a, b**) Immunostaining and Western blot showing the expression of tau P301S and tau P301SN255AN368A in mice brain. Scale bar, 50 μm. (**c**) Electron microscopy of the synapses. Arrows indicate the synapses. Scale bar, 1 μm. (**d**) Quantification of synaptic density (mean ± SEM; $n = 6$; $^{*}P < 0.05$, $^{**}P < 0.01$, one-way ANOVA). (**e**) The ratio of paired pulses is greater in tau P301SN255AN368A mice than in tau P301S mice (mean ± SD; $n = 6$ in each group; $^{*}P < 0.05$, one-way ANOVA). (**f**) LTP of fEPSPs (mean ± SD; $n = 6$ in each group; $^{*}P < 0.05$, one-way ANOVA). Shown traces are representative fEPSPs recorded at the time point 1 and 2 (tau P301S), 3 and 4 (tau P301SN255AN368A). (**g**) I/O curves obtained in hippocampal slices prepared from mice injected with AAV-GFP control, AAV-tau P301S, and AAV-tau P301SN255AN368A. (**h**) Averaged slope of I/O curves (mean ± SD; $n = 6$; $^{*}P < 0.05$, one-way ANOVA). (**i**) Morris water maze analysis as time to platform (sec) and integrated latency (AUC) for mice injected with AAV-GFP control, AAV-tau P301S, or AAV-tau P301SN255AN368A (mean ± SEM; $n = 10$; $^{**}P < 0.01$, one-way ANOVA). (**j**) Probe trail result (left panel, mean ± SEM; $n = 10$; $^{*}P < 0.05$, $^{**}P < 0.05$, one-way ANOVA). The swim speed of the mice was not affect by the expression of tau P301S or tau P301SN255N368 (right panel, mean ± SEM; $n = 10$; $P = 0.512$, one-way ANOVA).